Analysis of the Backscatter Spectrum in an Ionospheric Modification Experiment

by

H. Kim, F. W. Crawford, and K. J. Harker

December 1974

NASA Grant NGL 05-020-176

SU-IPR Report No. 609

INSTITUTE FOR PLASMA RESEARCH
STANFORD UNIVERSITY, STANFORD, CALIFORNIA

ANALYSIS OF THE BACKSCATTER SPECTRUM IN AN IONOSPHERIC MODIFICATION EXPERIMENT

by

H. Kim, F. W. Crawford, and K. J. Harker

NASA Grant NGL 05-020-176

SU-IPR Report No. 609

December 1974

Institute for Plasma Research
Stanford University
Stanford, California 94305

ANALYSIS OF THE BACKSCATTER SPECTRUM IN AN IONOSPHERIC MODIFICATION EXPERIMENT

by

H. Kim, F. W. Crawford, and K. J. Harker
Institute for Plasma Research
Stanford University
Stanford, California

ABSTRACT

The purpose of this study is to compare predictions of the backscatter spectrum, including effects of ionospheric inhomogeneity, with experimental observations of incoherent backscatter from an artificially heated region. Our calculations show that the strongest backscatter echo received is not from the reflection level, but from a region some distance below (about 900 m for an experiment carried out at Arecibo). By taking the standing wave pattern of the pump into account properly, the present theory explains certain asymmetrical features of the up-shifted and down-shifted plasma lines in the backscatter spectrum, and the several satellite peaks typically accompanying them.

CONTENTS

		Page
	ABSTRACT	ii
	LIST OF FIGURES	iv
1.	INTRODUCTION	1
2.	INCOHERENT SCATTERING REGIONS	5
3.	SCATTERED SPECTRUM INTENSITY	10
4.	ASYMMETRY OF THE LINES	17
5.	FREQUENCY DISPLACEMENTS	18
6.	CONCLUSION	24
	REFERENCES	25

LIST OF FIGURES

Page

Fig. 1. Backscatter spectrum obtained at Arecibo. (Δf is frequency displacement of up-shifted line from $f_i + f_0$, and of down-shifted line from $f_i - f_0$; f_i = 430 MHz; ordinary mode pump wave, f_0 = 5.62 MHz. After Kantor, 1974) 2

Fig. 2. Diurnal variations of frequency displacements. (The figure contains data obtained between May 1971 and March 1972. The bars represent the range of all available data for one hour intervals. After Kantor, 1974) 3

Fig. 3. Three-wave interactions of backscatter (dashed parallelograms) and heating (solid parallelograms). (a) The incident UHF waves (ω_{i1} and ω_{i2}) scatter off upward-propagating ($\omega_{\ell 1}$, $k_{\ell 1} > 0$) and downward-propagating ($\omega_{\ell 2}$, $k_{\ell 2} < 0$) Langmuir waves (L), at the same height, to give down-shifted (ω_D) and up-shifted (ω_U) lines 6

(b) The incident UHF wave (ω_i) scatters off an upward-propagating Langmuir wave ($\omega_{\ell 1}$, $k_{\ell 1} > 0$) to give a down-shifted line (ω_D), at a height above that at which it scatters off a downward-propagating Langmuir wave ($\omega_{\ell 2}$, $k_{\ell 2} < 0$) to give an up-shifted line (ω_U) 7

Fig. 4. Swelling factor for $|R| = 3^{-1/2}$ and $\psi = 0$ as function of z/h_0. [The frequency scales are obtained from (6).] 13

Fig. 5. Backscatter spectra.

(a) $\psi = -\pi/2, 0$ 15

(b) $\psi = \pi/2, \pi$ 16

Fig. 6. Swelling factor, S_0, and Function F 20

List of Figures (Contd.)

Page

Fig. 7. Variation of frequency shift with phase of reflection coefficient 21

Fig. 8. Frequency displacements of plasma lines [Schematic. Four values of swelling factor indicated in (a) are all at $\Delta f = f_a$. In (b) and (c), swelling factors for up-shifted (S_U) and down-shifted (S_D) lines near $\Delta f = f_a$ are approximated by straight lines.] 23

1. Introduction

From experimental results obtained at Arecibo (Carlson, Gordon and Showen, 1972; Kantor, 1974), it is believed that the enhanced heating and anomalous absorption occurring in the ionosphere are mainly due to parametric decay instabilities: the HF ordinary (pump) wave supplied by a high power transmitter ($\sim$ 100 kW), and propagating in the F-layer, decays into electron plasma and ion acoustic waves to enhance the plasma fluctuations (DuBois and Goldman, 1965; Nishikawa, 1968). Several analyses have been carried out of the saturation spectra in homogeneous (DuBois and Goldman, 1972a,b; Valeo, Oberman and Perkins, 1972; Kruer and Valeo, 1973; Harker, 1972; Kuo and Fejer, 1972; Fejer and Kuo, 1973; Perkins, Oberman and Valeo, 1974) and inhomogeneous (Arnush, Fried and Kennel, 1974) plasmas, with the assumption that the pump field is well above the threshold for parametric amplification. This results in saturation of the electron plasma waves due to nonlinear Landau damping by positive ions, or due to absorption caused by electrons whose orbits are nonlinearly perturbed by the waves (Bezzerides and Weinstock, 1972).

Some essential features of the backscatter spectrum are not fully understood yet, however. For example, Carlson et al. (1972) have obtained a pair of plasma lines in the spectrum enhanced by the pump wave (f_0 = 5.62 MHz). These plasma lines are shifted up and down from the incoherent scatter diagnostic beam (f_i = 430 MHz) by approximately $f_0 - f_a$, where $f_a (\approx 4$ kHz) is the frequency of the ion acoustic waves generated, and differ from each other in the intensities of the peaks (Figure 1). Kantor (1974) has further observed that this frequency displacement varies in time, but its difference for the up-shifted and the down-shifted lines is almost constant throughout the day, averaging 0.4 $\pm$ 0.1 kHz (Figure 2). As shown in Figure 1, he also observed several maxima and minima near the peaks of the spectrum. The purpose of this paper is to present a possible explanation of these features by considering the scattering region in relation to the Airy function form of the pump field variation in an ionosphere with an approximately linear density profile.

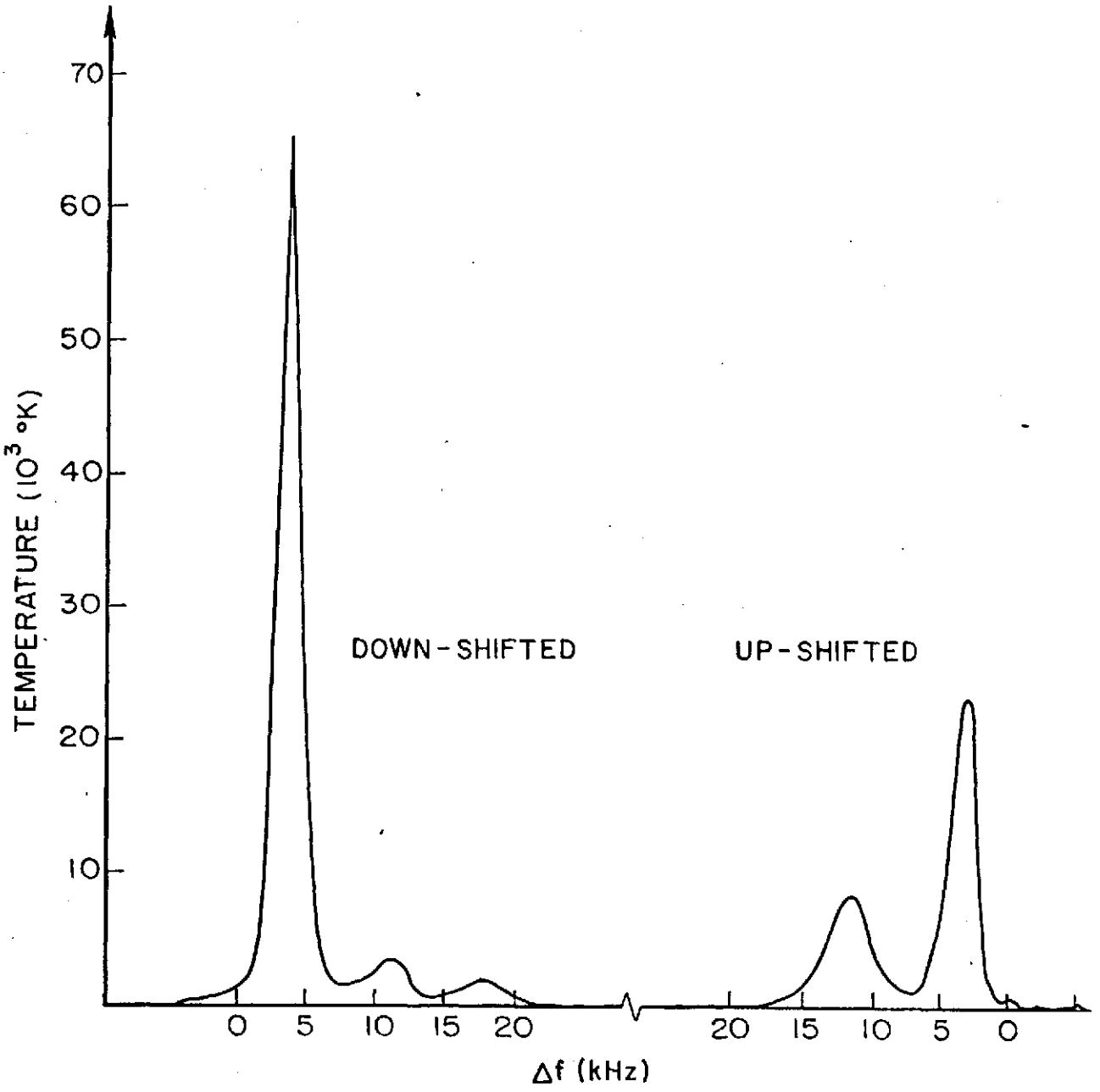

FIG. 1. Backscatter spectrum obtained at Arecibo. (Δf is frequency displacement of up-shifted line from $f_i + f_0$, and of down-shifted line from $f_i - f_0$; f_i = 430 MHz; ordinary mode pump wave, f_0 = 5.62 MHz. After Kantor, 1974).

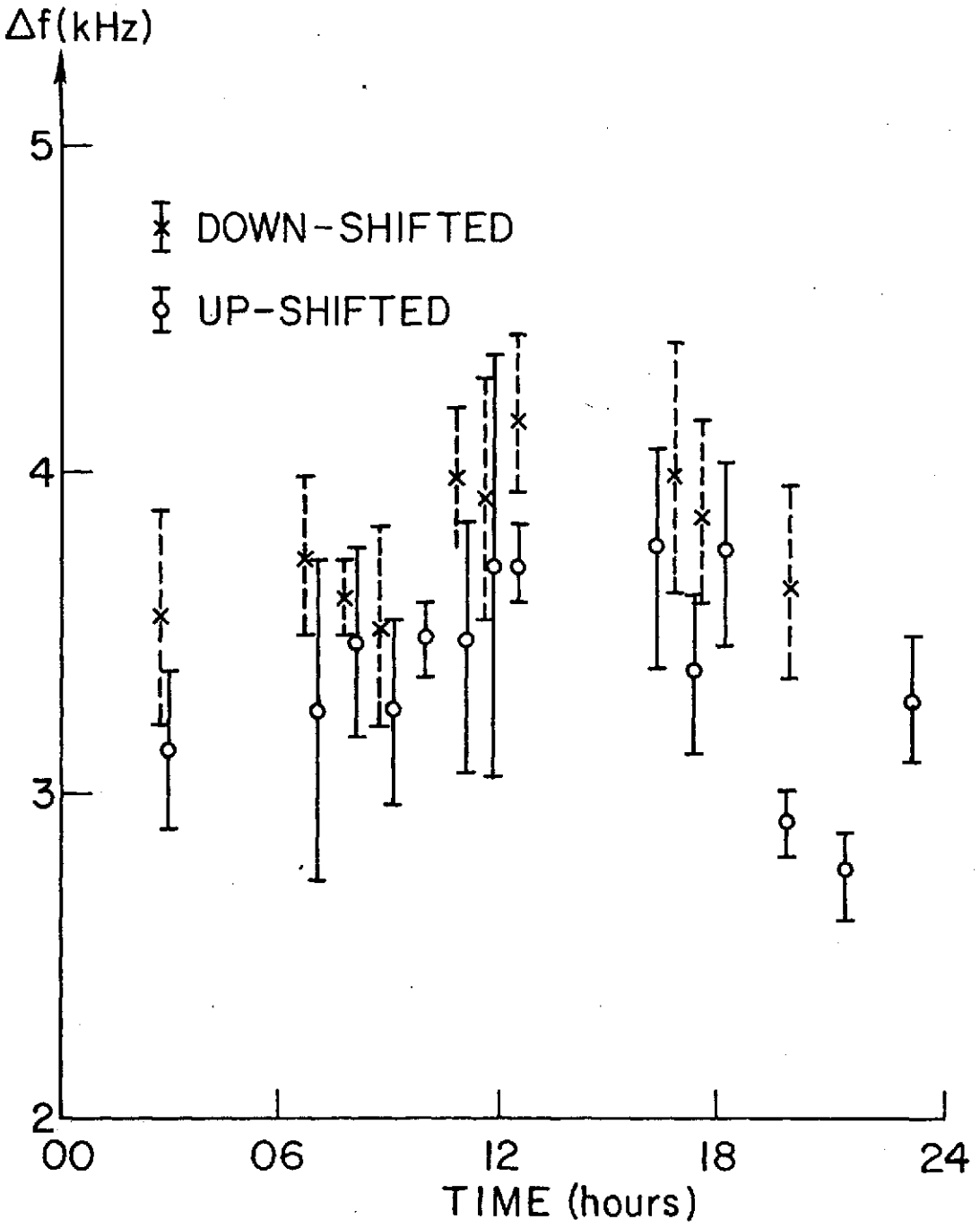

FIG. 2. Diurnal variations of frequency displacements. (The figure contains data obtained between May 1971 and March 1972. The bars represent the range of all available data for one hour intervals. After Kantor, 1974).

In regard to the asymmetry of the intensities, Fejer (1972) suggested that it is due to the convective amplification of upward- and downward-propagating plasma waves: those responsible for scattering the up-shifted and the down-shifted lines have been generated below and above the scattering height, respectively. This generation height difference was found to be nearly equal to the adjacent maximum-minimum distance of the pump amplitude. Following the estimate of Perkins et al. (1974), however, we neglect this convective amplification. Instead, we consider the small difference between the wave-numbers of the up-shifted and down-shifted lines, from which it is found that the asymmetry of the line intensities is due to the height difference of the scattering regions for the two lines: the up-shifted line is scattered in a region below that for the down-shifted, by about 1/10 of the distance of the adjacent maximum-minimum of the pump amplitude. It is further shown that the present analysis is consistent with Kantor's observations.

2. Incoherent Scattering Regions

As the pump wave from the HF transmitter propagates vertically upward in the ionosphere, its group velocity decreases very sharply near, and reaches zero at, the reflection level. Since more slowly moving waves spend a longer time in a given location, and are thus able to exchange energies more effectively, the decay of the pump wave (ω_0) into Langmuir (ω_ℓ) and ion acoustic (ω_a) waves occurs mainly near the reflection level. Figure 3(a) shows two possible synchronism parallelograms denoted by subscripts 1 and 2,

$$\omega_{\ell 1,2} = \omega_0 - \omega_{a1,2} \quad , \qquad k_{\ell 1,2} = k_{a1,2} \pm k_0 \quad , \tag{1}$$

where $k_0 \ll k_a, k_\ell$ and may thus be approximated to vanish near the reflection level, and (ω_ℓ, k_ℓ) and (ω_a, k_a) satisfy the dispersion relations

$$\omega_\ell^2 = \omega_p^2 \left(1 + 3\left(\frac{k_\ell}{k_d}\right)^2 + \left(\frac{\omega_c}{\omega_p}\right)^2 \sin^2\Theta\right) \quad , \qquad \omega_a = k_a v_a \ . \tag{2}$$

Here k_d is the electronic Debye wave-number: ω_c is the angular cyclotron frequency; Θ is the angle between $\underline{k}_\ell$ and the geomagnetic field; and the acoustic speed is given by $v_a = \alpha[(3\Theta_e + \Theta_i)/m]^{1/2}$, where α is the square root of the ion/electron mass ratio, m is the electron mass and $\Theta_{e,i}$ are the electron and ion temperatures in energy units.

At Arecibo, the intensity of this enhanced Langmuir wave is measured by sending a diagnostic wave vertically and determining its scattering intensity. Figure 3(a) illustrates the scattering synchronism conditions among the incident (ω_i), the scattered (down-shifted, ω_D, and up-shifted, ω_U), and the Langmuir (ω_ℓ) waves,

$$\omega_{D,U} = \omega_{i1,2} \mp \omega_{\ell 1,2} \quad , \qquad k_{D,U} = k_{\ell 1,2} - k_{i1,2} \ . \tag{3}$$

The dispersion relations for scattered and incident waves can be approximated by $\omega = kc$, where c is the speed of light.

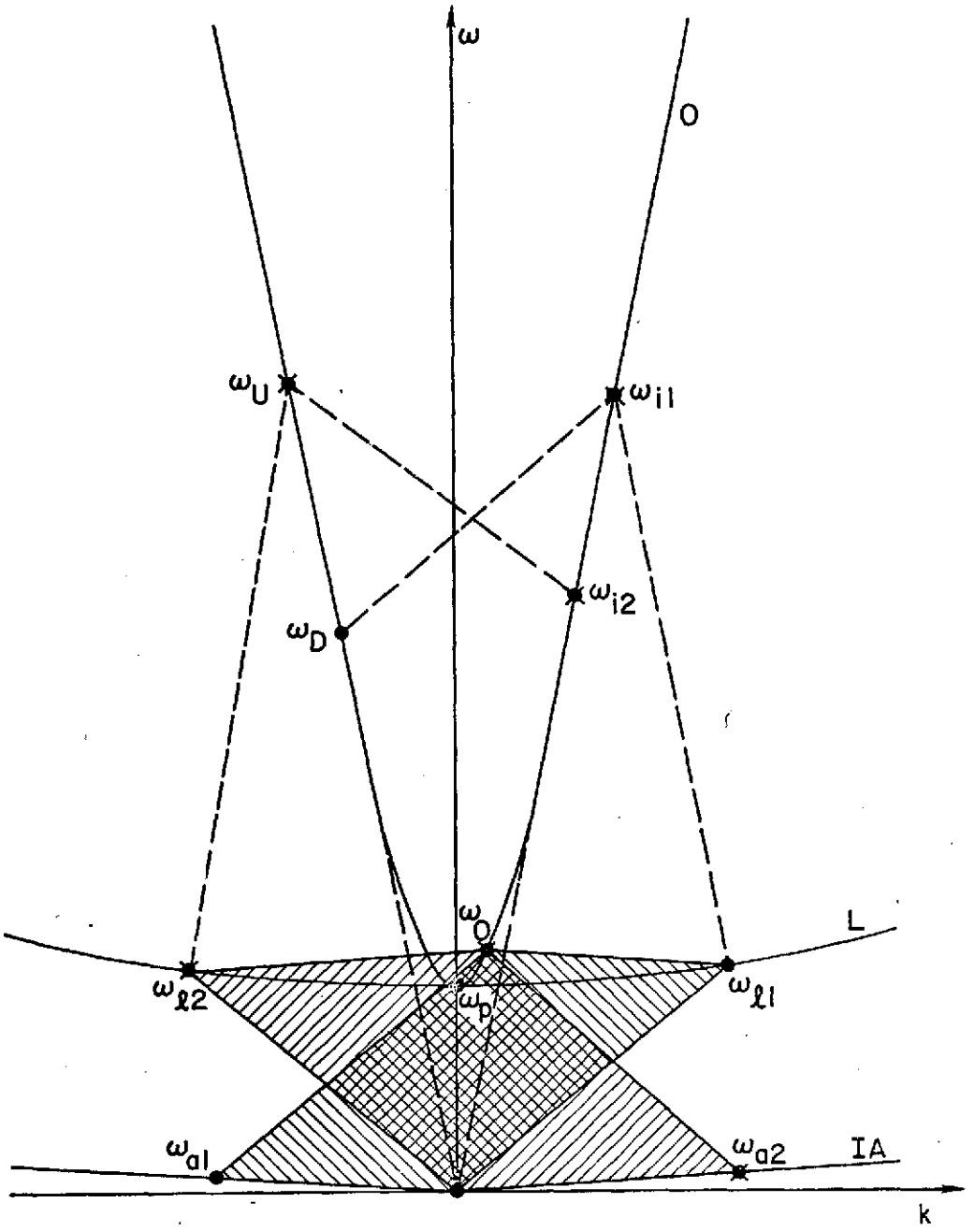

FIG. 3. Three-wave interactions of backscatter (dashed parallelograms) and heating (solid parallelograms).
(a) The incident UHF waves (ω_{i1} and ω_{i2}) scatter off upward-propagating ($\omega_{\ell 1}$, $k_{\ell 1} > 0$) and downward-propagating ($\omega_{\ell 2}$, $k_{\ell 2} < 0$) Langmuir waves (L), at the same height, to give down-shifted (ω_D) and up-shifted (ω_U) lines.

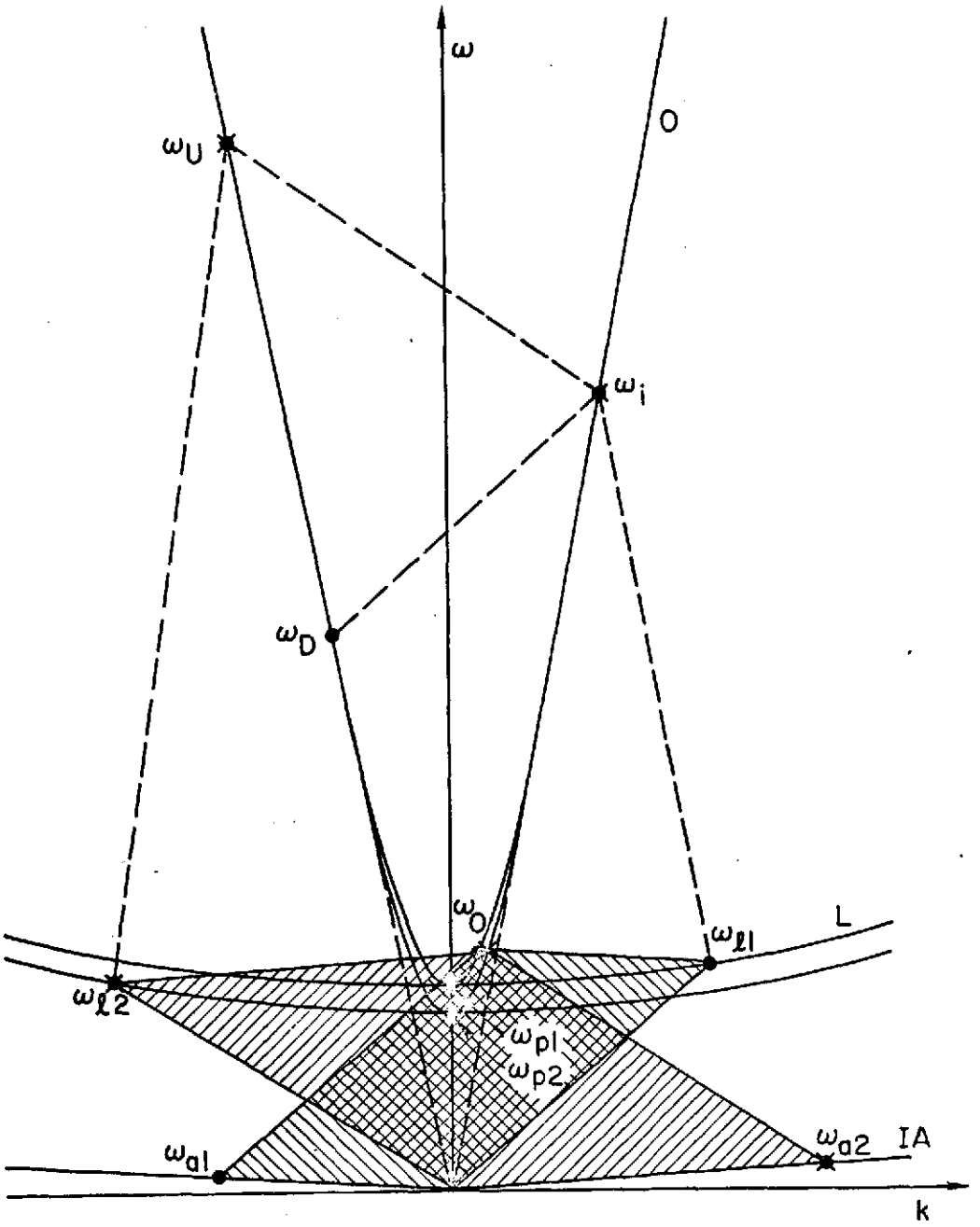

FIG. 3. Three-wave interactions of backscatter (dashed parallelograms) and heating (solid parallelograms). (b) The incident UHF wave (ω_i) scatters off an upward-propagating Langmuir wave (ω_{l1}, $k_{l1} > 0$) to give a down-shifted line (ω_D), at a height above that at which it scatters off a downward-propagating Langmuir wave (ω_{l2}, $k_{l2} < 0$) to give an up-shifted line (ω_U).

Figures 1 and 2 are drawn against $\Delta f \equiv f_D - (f_i - f_0)$ for the down-shifted and $\Delta f \equiv (f_i + f_0) - f_U$ for the up-shifted lines. If we neglect for a moment the effects of off-synchronism and ionospheric inhomogeneity, the scattered waves peak when ω_D and ω_U meet the synchronism conditions (1) and (3), i.e., when $\Delta\omega = \omega_{a1,2}$. In order to obtain the value of ω_a, we first note that use of the dispersion relations of the scattered waves ($\omega = kc$) reduces (3) to

$$k_{\ell 1,2} = \frac{2\omega_{i1,2} \mp \omega_{\ell 1,2}}{c} \quad . \tag{4}$$

Since ω_ℓ [$\approx 2\pi \times (5.6$ MHz)] $\ll \omega_i$ [$= \omega_{i1} = \omega_{i2} \approx 2\pi \times (430$ MHz)] for the Arecibo experiment, we may drop ω_ℓ from (4). Therefore, $k_{\ell 1} \approx k_{\ell 2}$. Assuming $k_0 \approx 0$ in (1), and using the ion acoustic wave dispersion relation in (2), reduces (4) to

$$\omega_{a1} \approx \omega_{a2} \approx \frac{2v_a}{c}\omega_i \quad . \tag{5}$$

For the temperature $T_e \approx T_i \approx 1200^\circ$ K and $\alpha \approx 1/170$, the scattered waves then peak at $\Delta f = f_{a1} \approx f_{a2} \approx 4$ kHz which agrees with Figure 1.

We now consider the effect of the second term on the RHS of (4). Due to the second term, $k_{\ell 1} \neq k_{\ell 2}$. The frequencies of the two Langmuir waves, on the other hand, are almost the same, $\omega_{\ell 1} \approx \omega_{\ell 2} = \omega_0 - \omega_a$ from (1) because $\omega_{a1} \approx \omega_{a2}$. Therefore, the up-shifted wave must be scattered at a height different from that for the down-shifted wave. This is illustrated in Figure 3(b). These two scattering heights can be obtained from the Langmuir wave dispersion relation (2) by assuming a linear electron density profile, $\omega_p^2 = \omega_0^2 z/h_0$, uniform geomagnetic field, and uniform electron temperature, and by substituting from (4) to obtain

$$\frac{z}{h_0} = \left(\frac{\omega_\ell}{\omega_0}\right)^2 - \left(\frac{\omega_c}{\omega_0}\right)^2 \sin^2\theta - \frac{12\omega_i(\omega_i \mp \omega_0)}{\omega_0^2}\left(\frac{v_e}{c}\right)^2 \quad . \tag{6}$$

Here, z is the height measured from the base of the ionosphere, h_0 is the scale height, and $v_e[=(\Theta_e/m)^{1/2}]$ is the electron thermal velocity. In the last term, $\omega_\ell = \omega_0$ is taken because $\omega_a \ll \omega_i$. For typical values in the Arecibo experiment of $f_0 = 5.62$ MHz, $f_c = 1.05$ MHz, $\theta = 40^\circ$, and $h_0 = 3 \times 10^4$ m, the up-shifted wave is scattered at about 900 m below the reflection height, and is at about 10 m above the height where the down-shifted wave is scattered. This height difference for the down and up-shifted waves may seem minor. As we shall see later, however, the intensity of the enhanced Langmuir wave is a sensitive function of height, and this small difference in height results in a considerable difference in the amplitudes of the down- and up-shifted spectra.

3. Scattered Spectrum Intensity

The power scattered by the enhanced Langmuir waves is given by (Harker, 1972)

$$dP_s = \frac{n_0 \sigma_T P_T A \eta}{(h+z)^2} \left(\frac{k_\ell}{k_{d0}}\right)^2 \left(\frac{\epsilon_0 I_k}{\Theta_e}\right) dz \ , \qquad (7)$$

where n_0 and k_{d0} are the local electron density and the Debye wavenumber at the reflection level, $\sigma_T (= 7.94 \times 10^{-30}\ m^2)$ is the Thompson backscattering cross-section, $P_T (= 2.5\ MW)$ is the diagnostic beam power, $A (= 150^2 \pi\ m^2)$ and $\eta (= 40\%)$ are the antenna aperture and efficiency, respectively, $h (= 150\ km)$ is the height of the base of the ionosphere from the ground, and I_k is the steady state spectral energy density of the Langmuir wave, which can be obtained from the well known kinetic wave equation of parametric interaction among the pump (ω_0), Langmuir (ω_ℓ), and ion acoustic (ω_a) waves. Changing variable z to ω_ℓ by (6), $dz/h_0 = 2\omega_\ell d\omega_\ell / \omega_0^2$, and substituting $dP_s/d\omega_\ell = K_B T_s / 2\pi$ and (4) into (7), gives

$$T_s = \frac{4\pi n_0 \sigma_T P_T A \eta\ h_0}{K_B c^2 k_{d0}^2} \left(\frac{\omega_\ell}{\omega_0^2}\right)\left(\frac{2\omega_i \pm \omega_\ell}{h+z}\right)^2 \left(\frac{\epsilon_0 I_k}{\Theta_e}\right), \qquad (8)$$

where K_B is Boltzmann's constant.

So far, we have considered the case where the synchronism condition (1) is met precisely. We will now include the effect of a slight frequency mismatch $\omega_\ell = \omega_0 - \omega_a + \delta\omega$. By neglecting higher order processes, such as nonlinear ion Landau damping or electron orbit perturbation, I_k may then be written in a simple form (Harker, 1972).

$$I_k = \left(\frac{\Theta_e k_d}{\epsilon_0 \alpha k_\ell}\right) PS\phi \cot^2\theta \ , \qquad (9)$$

where P and the resonance function ϕ are given by

$$P = \frac{\epsilon_0}{16 n_{0\textcircled{R}}} \left(\frac{\omega_\ell}{\gamma_e}\right) \left(\frac{\omega_0}{\omega_p}\right)^2 |E_0|^2 \quad , \quad \phi = \frac{1}{1 + (\delta\omega/\gamma_a)^2} \quad . \qquad (10)$$

Here, $\gamma_e (= 650/\text{sec})$ and $\gamma_a (= 8000\pi/\text{sec})$ are the linear damping rates of the electron plasma and ion acoustic waves, respectively, and E_0 is the pump field intensity at $z = 0$, which is given by

$$E_0 = \left(\frac{P_0 G}{\epsilon_0 \pi c h^2}\right)^{1/2} \quad , \quad G = \frac{4\pi A \eta}{c^2} f_0^2 \approx 130 \ , \qquad (11)$$

where P_0 is the HF pump power in watts, and G is the antenna gain.

All we need to know now is the swelling factor, S, in (9). Then, the RHS of (8) can be evaluated. In what follows, we neglect the geomagnetic field. After the pump field is found, however, it is regarded as being aligned in the direction of the geomagnetic field. In the absence of nonlinear absorption, the amplitude variation of a vertically propagating ordinary wave is customarily obtained by neglecting the Airy integral function, Bi, which grows with positive argument, because the field has to vanish as $z \to \infty$. The field is expressed by the decaying Airy integral function, Ai (Ginzburg, 1964; Budden, 1961). In the present situation, where most of the pump wave energy is deposited at or near the reflection level, however, we assume that the electric field vanishes for $z \geq h_0$ due to absorption, and phenomenologically keep the Bi term in the region below the reflection level ($0 \leq z \leq h_0$). In circuit terminology, this is analogous to a transmission line with a dissipative terminal impedance at $z = h_0$, whereas the usual treatment is analogous to an infinitely long nonuniform line. The solution to the wave equation in the ionosphere is then obtained by a similar procedure to that used in the absence of nonlinear absorption (Ginzburg, 1964; Budden, 1961). We obtain

$$|E|^2 = S|E_0|^2 \quad , \qquad (0 < z < h_0) \quad ,$$

$$S = \pi\zeta_0^{1/2} \left| \left\{ \exp\left[-i\left(\frac{2}{3}\,\zeta_0^{3/2} - \frac{\pi}{4}\right)\right] + R\,\exp\left[i\left(\frac{2}{3}\,\zeta_0^{3/2} - \frac{\pi}{4}\right)\right] \right\} \mathrm{Ai}(-\zeta) \right.$$

$$\left. + \left\{ \exp\left[-i\left(\frac{2}{3}\,\zeta_0^{3/2} + \frac{\pi}{4}\right)\right] + R\,\exp\left[i\left(\frac{2}{3}\,\zeta_0^{3/2} + \frac{\pi}{4}\right)\right] \right\} \mathrm{Bi}(-\zeta) \right|^2 \quad , \qquad (12)$$

where the effective reflection coefficient, R, is measured at $z = 0$, and ζ and ζ_0 are defined by

$$\zeta = \zeta_0\left(1 - \frac{z}{h_0}\right) \quad , \qquad \zeta_0 = \left(\frac{\omega_0 h_0}{c}\right)^{2/3} \quad . \qquad (13)$$

The familiar results for S and R in the absence of the absorbing layer are recovered from (12) by letting the Bi term equal zero (Ginzburg, 1964; Budden, 1961), as

$$S = 4\pi\zeta_0^{1/2}\,\mathrm{Ai}^2(-\zeta) \quad , \qquad R = \exp\left[-i\left(\frac{4}{3}\,\zeta_0^{3/2} - \frac{\pi}{2}\right)\right] . \qquad (14)$$

Our interests are in the scattering region. In this region $|\zeta| \gg 1$ and (12) becomes

$$S = \left(\frac{\zeta_0}{\zeta}\right)^{1/2} \left\{ 1 + |R|^2 + 2|R| \cos\left[\frac{4}{3}\left(\zeta_0^{3/2} - \zeta^{3/2}\right) + \psi\right] \right\} \quad , \qquad (15)$$

where ψ is the phase of the reflection coefficient. The swelling factor is plotted in Figure 4 for $|R| = 3^{-1/2}$ and $\psi = 0$.

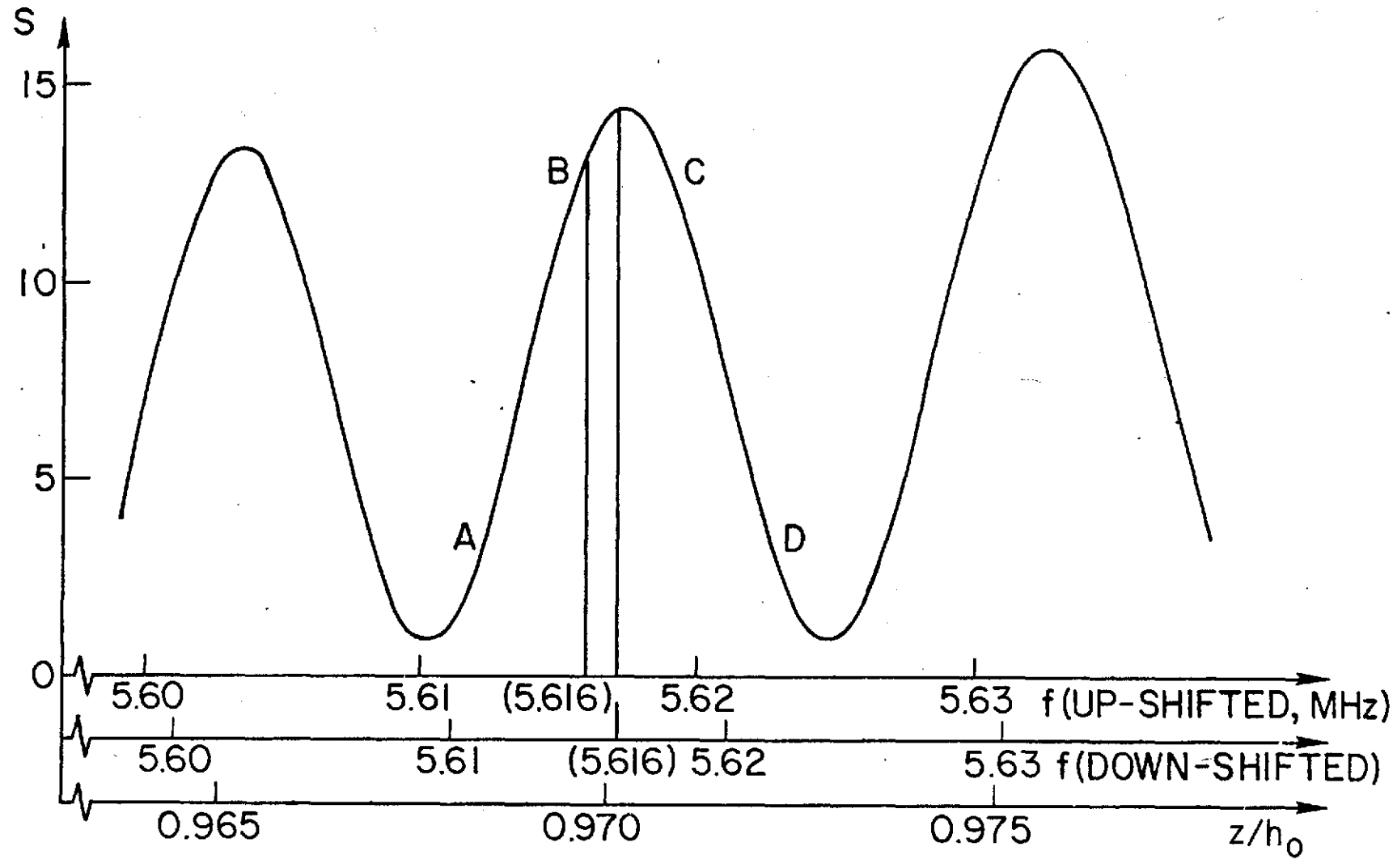

FIG. 4. Swelling factor for $|R| = 3^{-1/2}$ and $\psi = 0$ as function of z/h_0. [The frequency scales are obtained from (6)].

Now, the temperature spectrum (8) can be evaluated by substituting from (9)-(11) and (15). Here, we note that I_k in (9) is a function of z primarily through k_d/k, P, and S. Again changing variable z to ω_ℓ by (6), T_s is a function of f only. The spectrum is plotted against $\Delta f(\equiv f_0 - f)$ in Figure 5, with the phase of the reflection coefficient as a parameter.

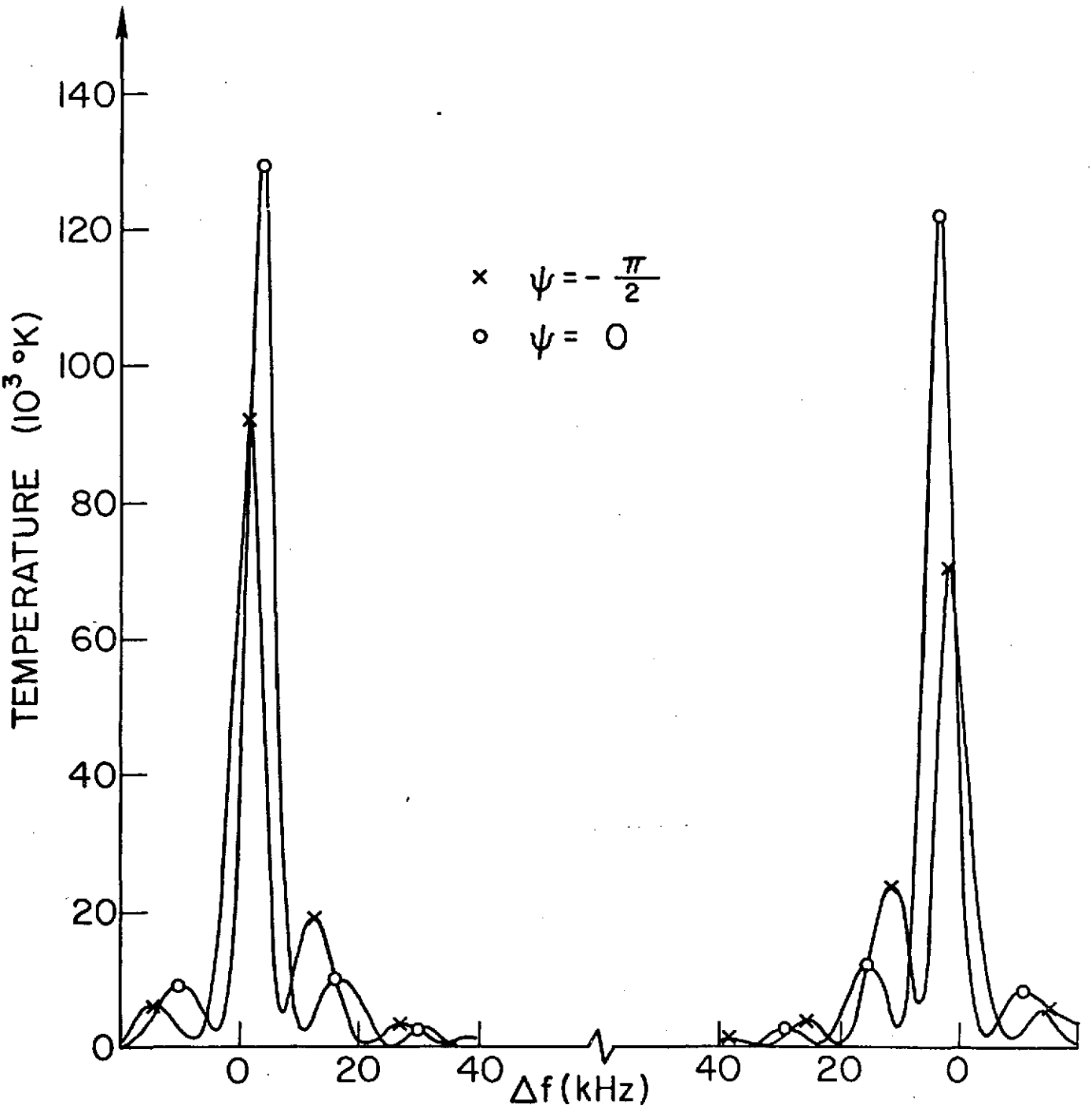

FIG. 5. Backscatter spectra. (a) $\psi = -\pi/2, 0$.

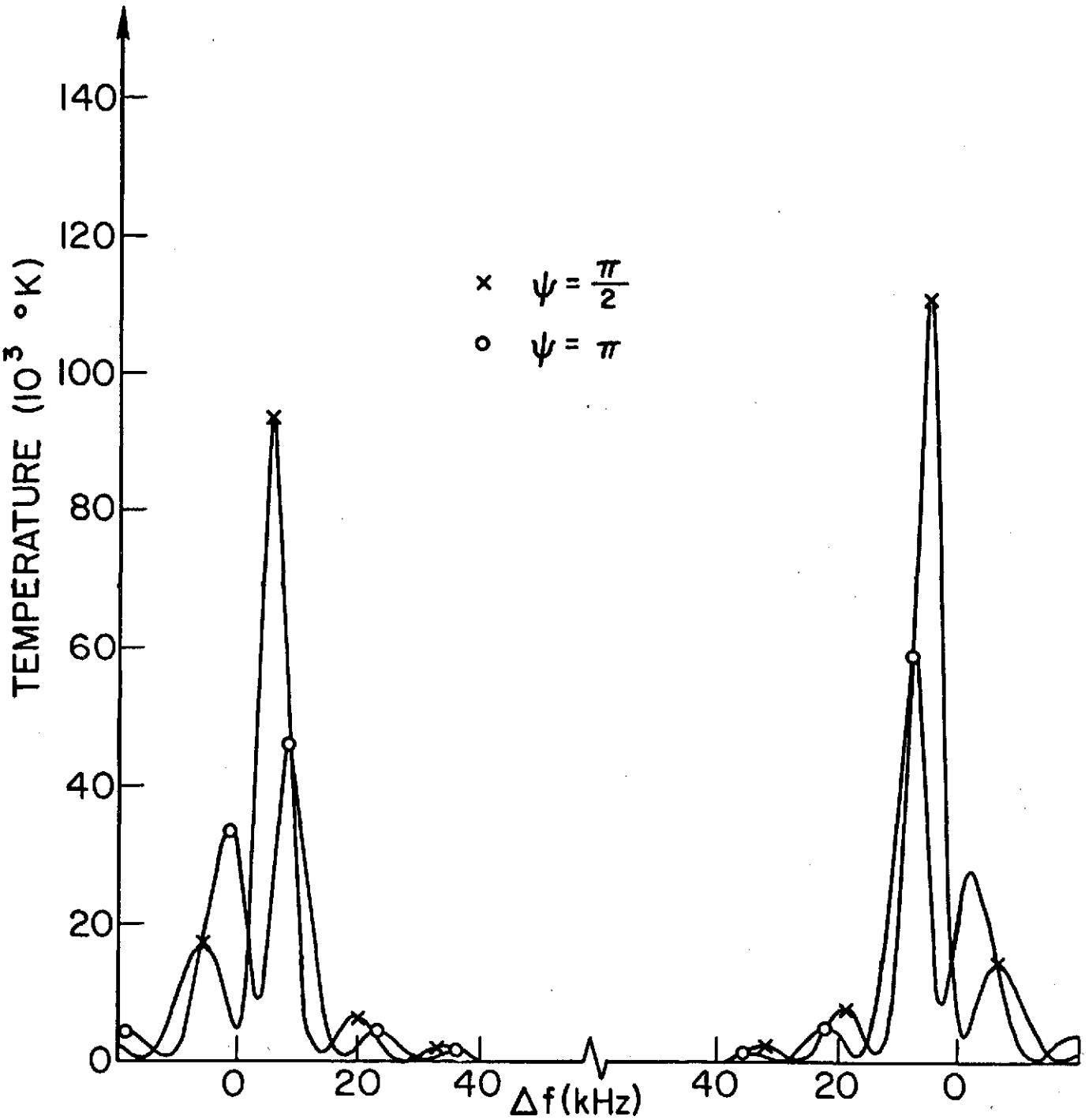

FIG. 5. Backscatter spectra. (b) $\psi = \pi/2, \pi$.

4. Asymmetry of the Lines

The spectra in Figure 5(a) show an overall agreement with the experimental results of Figure 1. Each spectrum has peaks near $\Delta f = f_a = 4$ kHz where the frequencies match precisely ($f = f_0 - f_a$). These peaks are due to electron plasma waves parametrically enhanced by the pump wave. The peak temperatures [$(6 \sim 13) \times 10^4$ °K] are in the range of experimental values [Kantor, 1974]. There are several maxima and minima near the peak of each spectrum. These are due to the swelling factor. The frequency intervals between adjacent maxima ($10 \sim 14$ kHz) are in good agreement with the experimental results in the range $8 \sim 18$ kHz (Kantor, 1974, Figures 3 and 5). The intensities of the up-shifted and down-shifted peaks differ from each other. This is due to the 10 m difference in heights (about 1/10 of the distance of the adjacent maximum-minimum of the swelling factor) where the scattered waves of $f = f_0 - f_a$ are generated, as calculated by (6). For $\psi = 0$, Figure 4 shows positive slopes of S at both heights. Since the down-shifted plasma line is scattered from a height higher than that for the up-shifted, the down-shifted line strength is higher than the up-shifted line, in agreement with the experimental results.

For $\psi = -\pi/2$, S shifts, and the heights for the down- and up-shifts are again on the positive slope somewhere between A and B in Figure 4 where the gradient of S is steeper. Therefore, the down-shifted line is stronger than the up-shifted again, but the difference in strength is greater than for $\psi = 0$. Figure 5(a) shows this difference as about 25% of the up-shifted line amplitude, which is much smaller than that shown in Figure 1. However, it depends on the strength of the up-shifted line in a quite involved way and most of the experimental data indicate smaller differences than that shown in Figure 1. [See Kantor (1974, Figure 9) and Carlson (1972, Figures 6 and 7)].

For $\psi = \pi/2$ and π, on the other hand, the heights for the down- and up-shifted lines are on the negative slope somewhere between C and D in Figure 4. The down-shifted peaks are therefore lower in amplitude than the up-shifted, as shown in Figure 5(b).

5. Frequency Displacements

Since we expect the peak of the spectrum to occur when I_k is a maximum, we can estimate the displacements of the plasma line frequencies from the pump frequency, Δf, from (9). Now I_k is maximum when $S\phi$ takes its maximum value. This occurs when $d(S\phi)/d\omega_\ell = 0$. Use of (10) then gives

$$\frac{1}{S}\frac{dS}{d\omega_\ell} \approx \frac{2\delta\omega}{\gamma_a^2} \quad . \tag{16}$$

We now expand S about the frequency precisely satisfying the synchronism condition (1), i.e., $\delta\omega = 0$.

$$S = S_0 + \frac{dS_0}{d\omega_\ell}\delta\omega + \frac{1}{2}\frac{d^2S_0}{d\omega_\ell^2}\delta\omega^2 + \ldots \quad . \tag{17}$$

To first order in $\delta\omega$, (16) then gives

$$\delta\omega = \frac{\frac{1}{S_0}\frac{dS_0}{d\omega_\ell}}{\frac{2}{\gamma_a^2} - \frac{d}{d\omega_\ell}\left(\frac{1}{S_0}\frac{dS_0}{d\omega_\ell}\right)} \quad . \tag{18}$$

Since ω_ℓ is related to z through (6), $d(z/h_0)/d\omega_\ell = 2\omega_\ell/\omega_0^2 \approx 2/\omega_0$, the frequency displacement of the Langmuir wave from the pump frequency, $\Delta\omega \equiv \omega_0 - \omega_\ell = \omega_a - \delta\omega$, becomes

$$\Delta\omega = \omega_a - \frac{(\gamma_a^2/\omega_0)S_0'/S_0}{1 - 2(\gamma_a/\omega_0)^2(S_0'/S_0)} \quad , \tag{19}$$

where the prime represents a derivative with respect to z/h_0.

Now consider the dependence of $\Delta\omega$ on ψ from (19). All we need to know is the behavior of S_0'/S_0. Since S_0 varies with z primarily through the cosine function in (15), for $|R| = 3^{-1/2}$,

$$\frac{S_0'}{S_0} = -\Psi' F(\Psi) \quad , \qquad F(\Psi) \equiv \frac{\sin\Psi}{2/3^{1/2} + \cos\Psi} \quad , \tag{20}$$

where $\Psi \equiv 4(\zeta_0^{3/2} - \zeta^{3/2})/3 + \psi$ is the argument of the cosine function in (15), and its (z/h_0)-derivative is $\Psi' = (2\omega_0 h_0/c)(1 - z/h_0)^{1/2}$. Since the variation of Ψ' with respect to z is negligible, differentiating (20) once again gives

$$\left(\frac{S_0'}{S_0}\right)' = -\Psi'^2 \frac{dF}{d\Psi} . \tag{21}$$

The function F is shown in Figure 6 in relation to S_0, the origin being chosen so as to make ψ the abscissa. Except near the minima of S_0, which are not of interest because of the small pump amplitude, F is nearly linear with ψ, with slope about 1/2. For $h_0 - z \approx 900$ m, $\Psi - \psi \approx 746 \times 2\pi - 0.3$ and therefore F may be approximated as

$$F \approx \frac{1}{2}(\psi - 0.3) \quad , \quad (\text{for } |\psi| < 0.8\pi) . \tag{22}$$

Since $\Psi' \approx 1224$, (20) and (21) reduce to

$$\frac{S_0'}{S_0} \approx -612(\psi - 0.3) \quad , \quad \left(\frac{S_0'}{S_0}\right)' \approx -7.5 \times 10^5 . \tag{23}$$

Equation (19) therefore becomes

$$\Delta f \approx \psi + 3.7 \text{ kHz} . \tag{24}$$

We now see from (23) and (24) and from Figure 6 that, for $-\pi < \psi \leq 0.3$, the slope of S_0 is positive and $\Delta f < 4$ kHz. For $0.3 < \psi \leq \pi$, on the other hand, S_0 has negative slope and $\Delta f > 4$ kHz.

Figure 7 shows Δf from (24), and more accurate numerical values for $\psi = -\pi/2$, 0 and $\pi/2$ obtained from Figure 5. These show that our results are in good agreement with Kantor's observation $\Delta f = 3 \sim 4$ kHz when $-\pi/4 \leq \psi \leq 0$, where the pump amplitude is nearly maximum and its slope is positive. It should also be noted that the

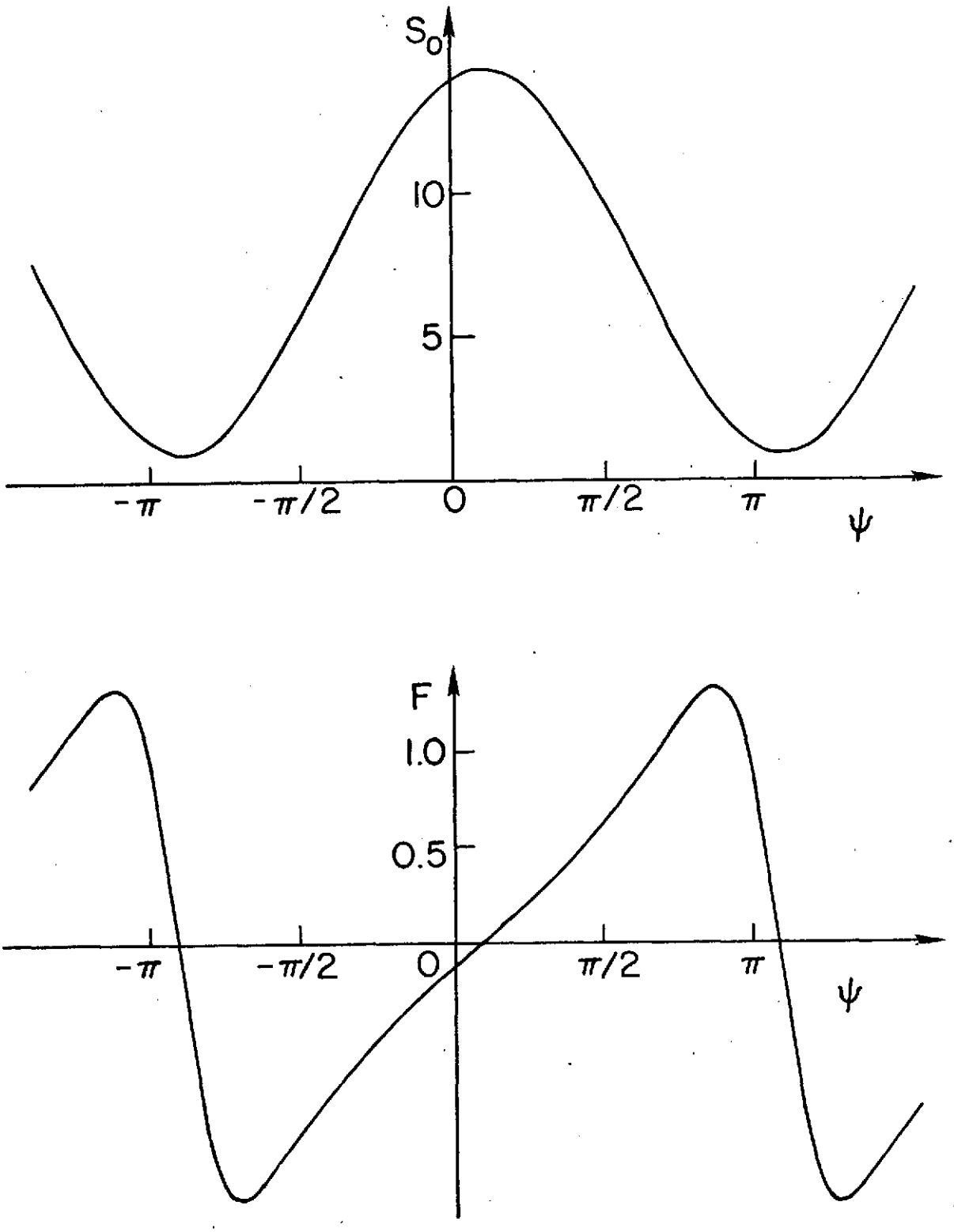

FIG. 6. Swelling factor, S_0, and Function F.

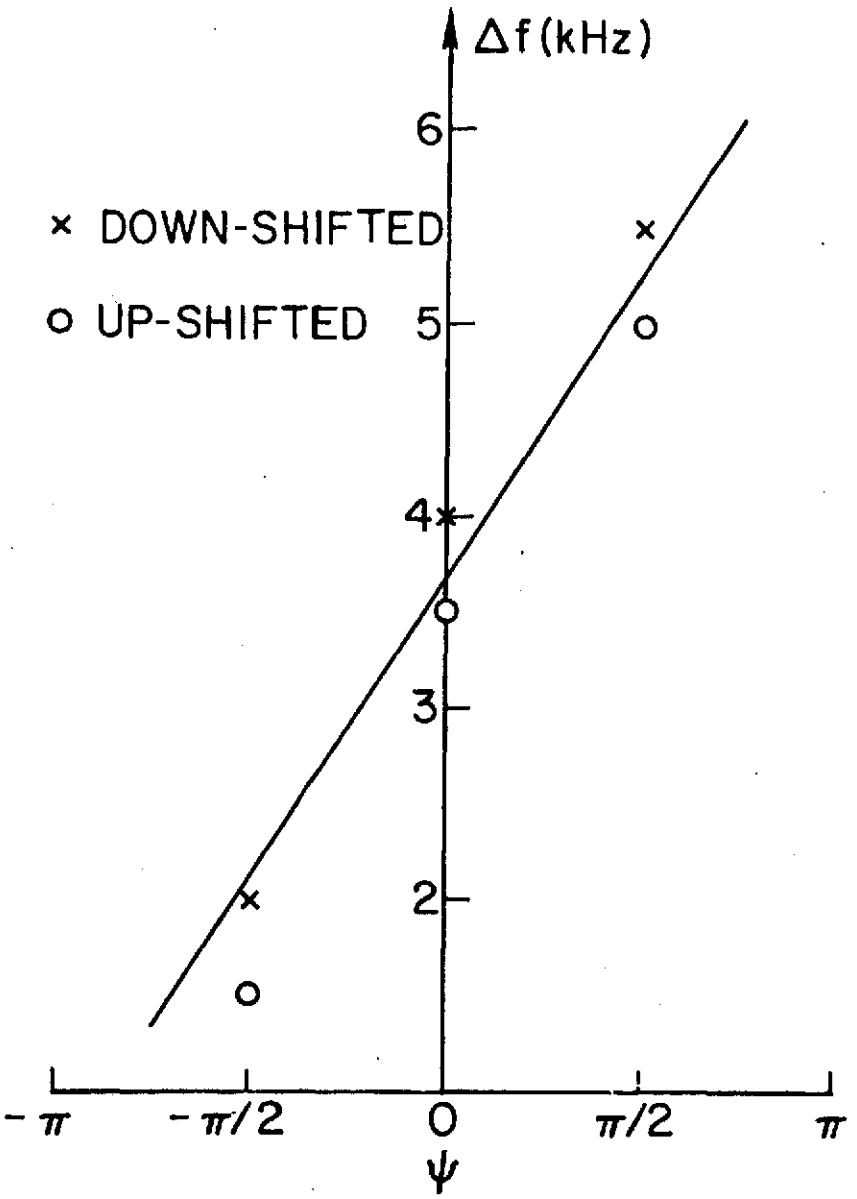

FIG. 7. Variation of frequency shift with phase of reflection coefficient.

frequency displacements of the down-shifted lines are always larger than those of the up-shifted, in agreement with the results of Kantor shown in Figure 2. The frequency difference is independent of ψ, with a value about 0.5 kHz. Again, this agrees with the experimental value of 0.4 ± 0.1 kHz.

The schematic diagram in Figure 8 offers a simple pictorial explanation for the larger displacements of the down-shifted lines than those of the up-shifted. We first note from (23) that S is convex throughout the region, except near its minima. Since slopes of S at the scattering heights are positive for $-\pi < \psi \leq 0.3$ and negative for $0.3 < \psi \leq \pi$, they may be drawn against Δf as in Figure 8(b) and (c). Note that, since $\Delta f = f_0 - f$, the slopes of S in (a) are reversed in (b) and (c). The figure also shows the resonance function ϕ peaking at $\Delta f = f_a$. Then, Δf of the peaks of the product ϕS increases or decreases from f_a, depending on the sign of the slope of S. The figure clearly demonstrates that, for both cases of (b) and (c), Δf of the peak of ϕS is larger for the down-shifted than for the up-shifted line.

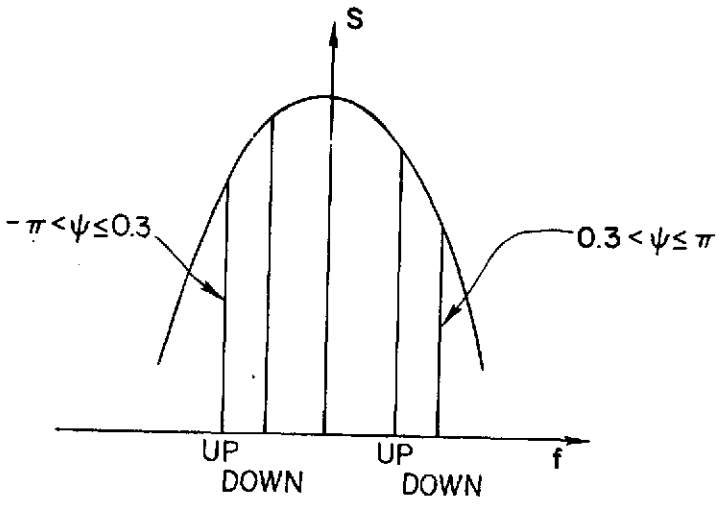

(a) SWELLING FACTOR

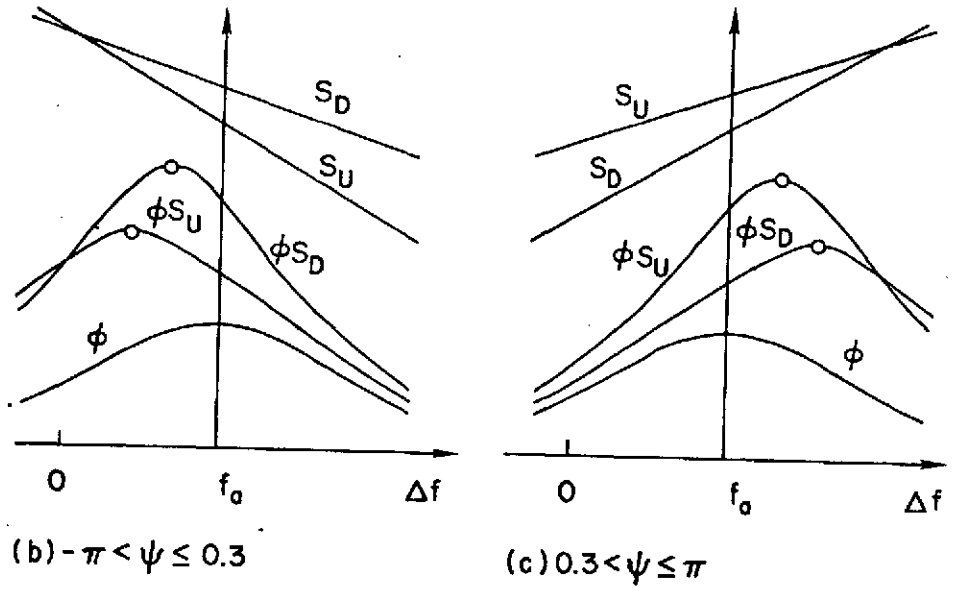

(b) $-\pi < \psi \leq 0.3$ (c) $0.3 < \psi \leq \pi$

FIG. 8. Frequency displacements of plasma lines [Schematic. Four values of swelling factor indicated in (a) are all at $\Delta f = f_a$. In (b) and (c), swelling factors for up-shifted (S_U) and down-shifted (S_D) lines near $\Delta f = f_a$ are approximated by straight lines.].

6. Conclusion

Since the scattered spectrum intensity is proportional to the pump field amplitude, the location where scattering occurs in relation to the standing wave pattern of the pump significantly affects the spectrum. Because of the random nature of the ionosphere, the peak amplitudes of the plasma lines and their frequency shifts vary widely with time. However, their average features agree well with the present theory if scattering occurs where the pump field is nearly maximum and its slope is positive. This happens when the phase of the reflection coefficient is confined within the range $\psi = -\pi/4 \approx 0$. It is therefore a subject of further experimental verification to establish whether ψ averaged over the time period of an observation is indeed near or within this range.

The several peaks in the region near the HF transmitter frequency have been explained previously as the transfer of power from one Langmuir wave to another at a slightly lower frequency via an ion acoustic beat wave (Kuo and Fejer, 1972, Kruer and Valeo, 1973; Fejer and Kuo, 1973). The present analysis shows, however, that the standing wave pattern of the pump wave can also result in these pumps. Further work is required to determine whether the peaks actually observed are due to the combined effects of the two mechanisms, or predominantly due to one of them.

Acknowledgement. This work was supported by the National Aeronautics and Space Administration.

REFERENCES

Arnush, D., B. D. Fried, and C. F. Kennel, Parametric amplification of propagating electron plasma waves in the ionosphere, J. Geophys. Res., 79, 1885, 1974.

Bekefi, G., Radiation Processes in Plasmas, John Wiley and Sons, New York, 1966.

Bezzerides, B., and J. Weinstock, Nonlinear saturation of parametric instabilities, Phys. Rev. Letters, 28, 481, 1972.

Budden, K. G., Radio Waves in the Ionosphere, Cambridge University Press, Cambridge, 1961.

Carlson, H. C., W. E. Gordon, and R. L. Showen, High frequency induced enhancements of the incoherent scatter spectrum at Arecibo, J. Geophys. Res., 77, 1242, 1972.

DuBois, D. F., and M. V. Goldman, Radiation-induced instability of electron plasma oscillations, Phys. Rev. Letters, 14, 544, 1965.

DuBois, D. F., and M. V. Goldman, Nonlinear saturation of parametric instability: Basic theory and application to the ionosphere, Phys. Fluids, 15, 919, 1972a.

DuBois, D. F., and M. V. Goldman, Spectrum and anomalous resistivity for the saturated parametric instability, Phys. Rev. Letters, 28, 218, 1972b.

Fejer, J. A., Variability of plasma-line enhancement in ionospheric modification experiments, J. Geophys. Res., 77, 273, 1972.

Fejer, J. A., and Y-Y. Kuo, Structure in the non-linear saturation spectrum of parametric instabilities, Phys. Fluids, 16, 1490, 1973.

Ginzburg, V. L., The Propagation of Electromagnetic Waves in Plasmas, Pergamon Press, Oxford, 1964.

Harker, K. J., Induced enhancement of the plasma line in the backscatter spectrum by ionospheric heating, J. Geophys. Res., 77, 6904, 1972.

Kantor, I. J., High frequency induced enhancements of the incoherent scatter spectrum at Arecibo, 2, J. Geophys. Res., 79, 199, 1974.

Kruer, W. L., and E. J. Valeo, Nonlinear evolution of the decay instability in a plasma with comparable electron and ion temperatures, Phys. Fluids, 16, 675, 1973.

Kuo, Y-Y., and J. A. Fejer, Spectral-line structures of saturated parametric instabilities, Phys. Rev. Letters, 29, 1667, 1972.

Nishikawa, K., Parametric excitation of coupled waves I. General formulation, J. Phys. Soc. Jap., 24, 916, 1968.

Perkins, F. W., C. Oberman, and E. J. Valeo, Parametric instabilities and ionospheric modification, J. Geophys. Res., 79, 1478, 1974.

Valeo, E., C. Oberman, and F. W. Perkins, Saturation of the decay instability for comparable electronic and ionic temperatures, Phys. Rev. Letters, 28, 340, 1972.